

Multimodal biometric method that combines veins, prints, and shape of a finger

Byung Jun Kang

Technical Research Institute
Hyundai Mobis
80-9 Mabook-dong
Giheung-gu, Yongin-shi
Gyunggi-do 446-912
Republic of Korea

Kang Ryoung Park

Dongguk University
Division of Electronics and Electrical Engineering
26, Pil-dong 3-ga
Jung-gu, Seoul 100-715
Republic of Korea
E-mail: parkgr@dongguk.edu

Jang-Hee Yoo

Jeong Nyeo Kim

Electronics and Telecommunications Research
Institute
138 Gajeongno Yuseong-gu
Daejeon, 305-700
Republic of Korea

Abstract. Multimodal biometrics provides high recognition accuracy and population coverage by using various biometric features. A single finger contains finger veins, fingerprints, and finger geometry features; by using multimodal biometrics, information on these multiple features can be simultaneously obtained in a short time and their fusion can outperform the use of a single feature. This paper proposes a new finger recognition method based on the score-level fusion of finger veins, fingerprints, and finger geometry features. This research is novel in the following four ways. First, the performances of the finger-vein and fingerprint recognition are improved by using a method based on a local derivative pattern. Second, the accuracy of the finger geometry recognition is greatly increased by combining a Fourier descriptor with principal component analysis. Third, a fuzzy score normalization method is introduced; its performance is better than the conventional Z-score normalization method. Fourth, finger-vein, fingerprint, and finger geometry recognitions are combined by using three support vector machines and a weighted SUM rule. Experimental results showed that the equal error rate of the proposed method was 0.254%, which was lower than those of the other methods. © 2011 Society of Photo-Optical Instrumentation Engineers (SPIE). [DOI: 10.1117/1.3530023]

Subject terms: multimodal biometrics; finger recognition; fuzzy score normalization.

Paper 100501RR received Jun. 21, 2010; revised manuscript received Nov. 18, 2010; accepted for publication Nov. 19, 2010; published online Jan. 24, 2011; corrected Jan. 26, 2011.

1 Introduction

Biometrics is a technology used to automatically identify individuals using physiological or behavioral features such as veins, fingerprints, irises, hand geometry, and faces. Conventional biometric systems that use a single biometric feature are disadvantaged in that their recognition capacities are limited by the degree of freedom of the biometric feature. Their performances are seriously affected by the conditions of the user's health, illumination, type of sensor, etc.¹ In a fingerprint recognition system, serious intrapersonal variations can arise from the humidity of the finger surface and skin distortions.^{2,3} The accuracy of a vein recognition system is reduced by changes in the vein thickness, which is related to the blood flow. A user's health and the weather conditions lead to variations in the blood flow.²⁻⁴ Multimodal biometric technology solves the problems of biometric systems that use only a single biometric feature.¹⁻⁵ Owing to the use of various biometric features obtained from multiple modalities, multimodal biometric technology has higher recognition accuracy than biometric systems that use a single biometric feature. This paper proposes a new finger recognition system based on the score-level fusion of various biometric features obtained from a single finger. A single finger contains several biometric features such as finger veins, the fingerprint, and the finger's geometric features. If multiple finger features are used for user authentication, high recognition accuracy and population coverage can be achieved in addition to avoiding the threat of spoofing.⁵

In previous works, many recognition approaches using the features of a single finger, such as fingerprint recognition,⁶⁻⁹ finger-vein recognition,¹⁰⁻¹² and finger geometry recognition^{2,3} have been introduced. There have also been studies that combined two biometric features of a finger to overcome the limitations of unimodal biometrics,^{2,3} but there have been no studies on the fusion of three features of a finger.

Ferrer et al. combined the hand vein and hand geometry features extracted by a 2D Gabor wavelet filter.¹³ However, the problem with this method was that the size of the capturing device was increased to acquire the hand features. To overcome this problem, Kang et al. introduced a multimodal biometric method based on the fusion of the finger geometry and finger-vein features.^{2,3} Lee et al. introduced the new device which can capture the finger vein and fingerprint images at the same time, but did not research the recognition algorithms of finger vein and fingerprint.¹⁵ In this paper, we propose a new finger recognition approach based on the fusion of the finger-vein, fingerprint, and finger geometry features in order to provide higher recognition accuracy and population coverage than the previous approaches that combined only two biometric features.

Lee et al. proposed a finger-vein recognition system based on the local binary pattern (LBP) method.¹⁰ In this study, we effectively extracted the finger-vein and fingerprint features by using a local derivative pattern (LDP) method. Because the LDP method can extract more elaborate and discriminative features than the LBP method,¹⁴ the LDP-based finger-vein and fingerprint recognition approaches perform better than the previous LBP-based approaches.^{10,11}

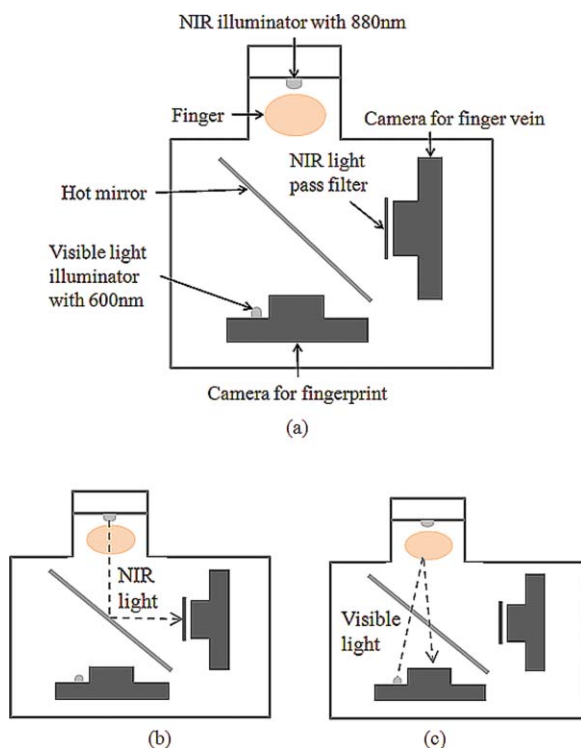


Fig. 1 Capturing device used to acquire the finger-vein and fingerprint images:¹⁵ (a) structure of the device; (b) path of the NIR light; and (c) path of the visible light.

The previous finger geometry recognition approach obtains finger shape representations based on the vertical thickness vectors of the finger region.² And the performance of the finger geometry recognition was enhanced by using the Fourier descriptor (FD) of the vertical thickness vectors of the finger region because the vertical thickness vectors are affected by the finger rotation, translation and segmentation error of finger region.³ However, there was a still problem that the performance of the finger geometry recognition is degraded because orthogonality between the FDs is not guaranteed.³ Therefore, we combined the FDs and principal component analysis (PCA) to guarantee the orthogonality; the subsequent performance of the finger geometry recognition was greatly improved.

The score-level fusion of the finger-vein, fingerprint, and finger geometry recognition was achieved by using three support vector machines (SVMs) and a weighted SUM rule after their scores were normalized by a fuzzy score normalization method. The proposed approach has a better performance than unimodal biometrics and the previous multimodal biometric methods.

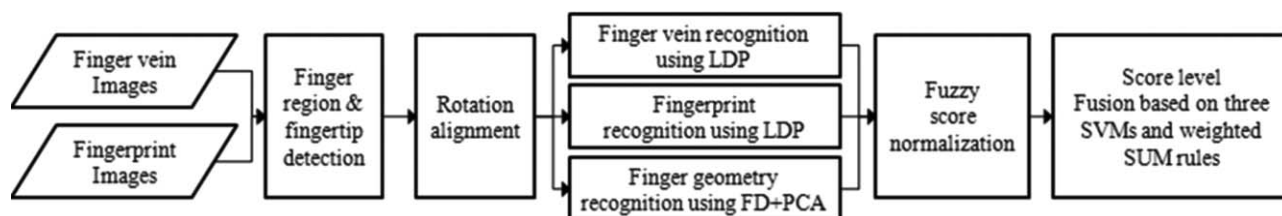


Fig. 2 Flowchart of the proposed multimodal biometric method combining the finger-vein, fingerprint, and finger geometry features.

The rest of this paper is organized as follows: Sec. 2 presents the proposed approach in detail, including descriptions of the LDP, FD, and PCA. The experimental results are explained in Sec. 3, and Sec. 4 summarizes our conclusions.

2 Proposed Multimodal Finger Recognition Method

2.1 Proposed Capturing Device

Figure 1 shows the structure for the capturing device to obtain the fingerprint, finger geometry, and finger-vein features of a single finger at the same time.¹⁵ A finger-vein image is acquired using near-infrared (NIR) light illumination because NIR light is absorbed into the hemoglobin and penetrates the skin of the finger.^{12,16} A fingerprint image can be obtained under visible light illumination because the fingerprint on the skin surface of the finger reflects visible light. In the capturing device, four 880-nm NIR light-emitting diodes (LEDs) and an NIR passing filter are used to acquire the finger-vein image, and a single 600-nm visible light LED is used for acquiring the fingerprint image. In order to reduce the size of the device, we used two conventional web cameras.¹⁷ For the camera used for the finger-vein image, the NIR blocking filter inside the camera was removed with the NIR passing filter attached to the front of the camera sensor. Because the camera used for the fingerprint image captures the image using visible light, it was left unaltered. In addition, the finger-vein and fingerprint images were simultaneously obtained from the two cameras by using a hot mirror that reflects the NIR light and transmits the visible light. Fig. 16 shows examples of the fingerprint and finger-vein images obtained from the capturing device.

2.2 Overview of the Proposed Approach

Figure 2 shows a block diagram illustrating the overall procedure of the finger recognition method that combines information from multiple biometric sources. Because the optical axis of the camera for the finger-vein image is in accordance with that of the camera for the fingerprint image based on the structure shown in Fig. 1,¹⁵ the finger is positioned at the same coordinates in the finger-vein and fingerprint images via an uncomplicated camera calibration. Thus, the position of the finger region in the fingerprint image is determined from the results of the finger detection in the finger-vein image. The finger-vein image is used for the finger detection because the fingerprint image includes a large amount of background noise at levels greater than those of the finger-vein image, as shown in Figs. 5(b) and 5(c). This is because the fingerprint image is captured under a visible light environment, and more noisy components in the background can be seen in visible light than in NIR light, as shown in Figs. 5(b) and 5(c).

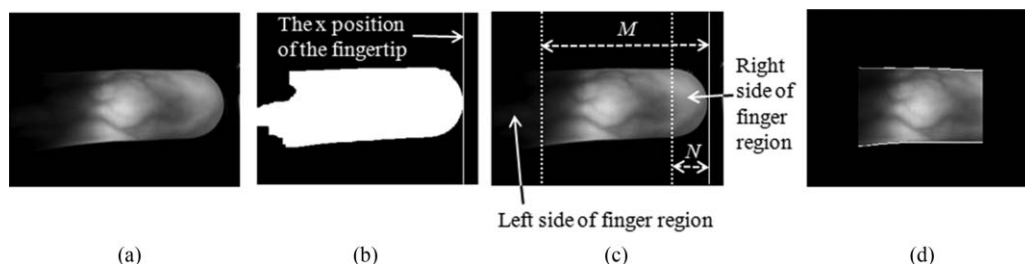


Fig. 3 Finger region and fingertip detection: (a) original finger-vein image; (b) result of the fingertip detection; (c) candidate area for the finger region detection; and (d) result of the finger region detection.

The finger region in the finger-vein image is found by detecting the horizontal edge lines between the finger and background; the fingertip is detected by image binarization. After measuring the angle between the x -axis and center line of the finger region, the rotation of the finger is aligned. Then, the three biometric features are extracted from a single finger as follows. The finger-vein and fingerprint features are extracted by the LDP. The finger geometry features are obtained by the method that combines the FD and PCA from the finger-vein image. The fuzzy membership scores are calculated by the predefined membership function by matching the scores of the three biometric features, and then, the user authentication is finally completed by fusion of the fuzzy scores using the three SVMs and the weighted SUM rule.

2.3 Finger Region and Fingertip Detection

Because the NIR light penetrates the finger skin, the finger skin shows higher intensity values than the background in a finger-vein image, as shown in Fig. 3(a). The finger region is less than 30% of the finger-vein image when the user's finger is located at the depth of focus region of the camera, so the brightest 30% of the pixels are assigned to 255 as the finger region. The remaining pixels in the background area are assigned to 0, as shown in Fig. 3(b). Because some of the background pixels can be set to 255 owing to ambient light and image noise, the largest region is found by component labeling; the x position of its right end point is then determined as the x position of the fingertip.

In order to detect the finger region in more detail, edge detection masks are used, as shown in Fig. 4. Because the NIR light barely penetrates through a thick finger, the finger-vein patterns are hard to separate from the finger skin on the left side of the finger region, as shown in Fig. 3(c). In addition,

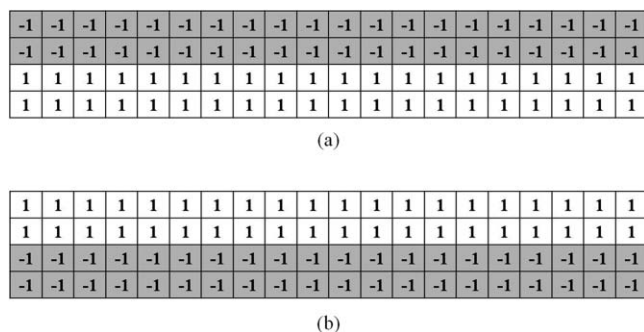


Fig. 4 Finger boundary detection mask: (a) detecting the upper boundary and (b) detecting the lower boundary.^{2,3}

the right side of the finger region rarely includes finger-vein patterns. Thus, the finger region is detected in the candidate area excluding the left and right sides of the finger region, as shown in Fig. 3(d). The M and N values are empirically set to 350 and 50 pixels, respectively, in the experiment.

2.4 Rotation Alignment

In order to reduce the recognition errors caused by rotation of the finger, a rotation alignment is carried out. The center line of the finger region is produced by calculating the mean values of the y positions of the upper and lower finger boundaries at each x position; the angle θ of the rotation is then determined by the Hough transform as

$$y = x \tan \theta + y_0, \tag{1}$$

where (x, y) and y_0 denote the points on the center line and the y position of the start point of the center line, respectively, as shown in Fig. 5(a). The start point is the location that is M pixels distant from the fingertip (x_{ft}), and the angle θ is constrained in the range of -30° to 30° for fast processing in consideration of the limitations on finger rotation in our device. Figs. 5(b) and 5(c) show the results of the rotation alignment.

2.5 Finger-Vein Recognition Based on LDP

The procedure for the finger-vein recognition is depicted in Fig. 6. The finger region is normalized into dimensions of 180×60 pixels to solve the problem of the size variations caused by the change in Z distance between the finger and camera. The size normalization is achieved by stretching the finger region horizontally and vertically; Fig. 7 shows some examples. To eliminate image noise and reduce the computational time, a subsampled image of 60×20 pixels is

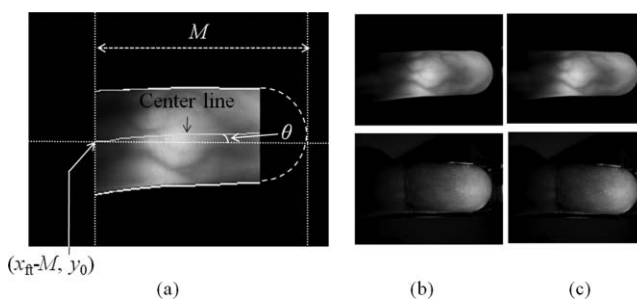


Fig. 5 Rotation alignment of a finger: (a) example of measuring the rotation angle from the center line; (b) original images; and (c) aligned finger-vein and fingerprint images.

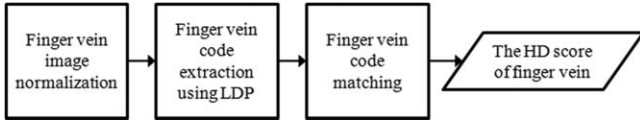


Fig. 6 Flowchart of the finger-vein recognition method.

obtained by selecting the mean gray value in every nonoverlapping block of 3×3 pixels within the normalized image.³

The LBP is the descriptor for representing the first-order derivative pattern;^{18,19} the LDP represents the high-order derivative pattern in a specific direction.¹⁴ Therefore, the LDP is reported to extract more elaborate and discriminative features than the LBP.¹⁴ In this paper, the finger-vein codes are extracted from the sub-sampled image by using a second-order LDP employed in the 0° , 45° , 90° , and 135° directions. If the eight adjacent pixels are located around I_c , as shown in Fig. 8, the first-order derivative bits along each direction are defined as

$$B_{0^\circ}(x_c, y_c) = f(I_4 - I_c), \quad (2)$$

$$B_{45^\circ}(x_c, y_c) = f(I_3 - I_c), \quad (3)$$

$$B_{90^\circ}(x_c, y_c) = f(I_2 - I_c), \quad (4)$$

$$B_{135^\circ}(x_c, y_c) = f(I_1 - I_c), \quad (5)$$

$$f(k) = \begin{cases} 1, & k > th \\ 0, & k \leq th \end{cases}, \quad (6)$$

where (x_c, y_c) and th denote the position of the center pixel I_c and the predefined threshold, respectively. The predefined threshold was set to 0 in our experiment. The LDP extracts the feature codes from the exclusive-OR (\otimes) operation of the corresponding first-order derivative bits between the center pixel and eight adjacent pixels.

$$LDP_\alpha(x_c, y_c) = \sum_{i=1}^8 \{B_\alpha(x_c, y_c) \otimes B_\alpha(x_c + u_i, y_c + v_i)\} \cdot 2^{i-1}, \quad (7)$$

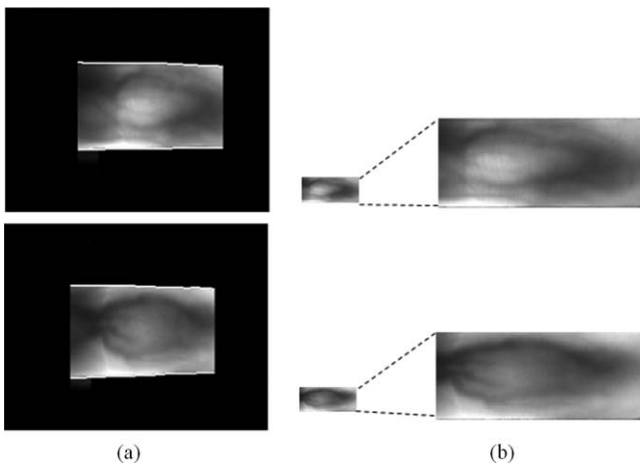


Fig. 7 Examples of the size normalization of the finger-vein image: (a) results of the finger detection and (b) subsampled images of 60×20 pixels.

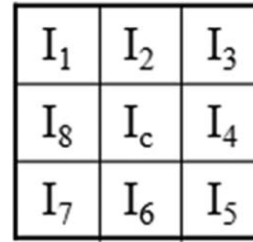


Fig. 8 Example of the eight adjacent pixels around I_c .

$$u_a = \begin{cases} -1, & \text{if } a = 1 \\ 0, & \text{if } a = 2 \\ 1, & \text{if } a = 3 \\ 1, & \text{if } a = 4 \\ 1, & \text{if } a = 5 \\ 0, & \text{if } a = 6 \\ -1, & \text{if } a = 7 \\ -1, & \text{if } a = 8 \end{cases}, \quad v_a = \begin{cases} -1, & \text{if } a = 1 \\ -1, & \text{if } a = 2 \\ -1, & \text{if } a = 3 \\ 0, & \text{if } a = 4 \\ 1, & \text{if } a = 5 \\ 1, & \text{if } a = 6 \\ 1, & \text{if } a = 7 \\ 0, & \text{if } a = 8 \end{cases}, \quad (8)$$

$$LDP_\alpha(x_c, y_c) = \{LDP_\alpha(x_c, y_c) \mid \alpha = 0^\circ, 45^\circ, 90^\circ, 135^\circ\}. \quad (9)$$

Figure 9 shows an example of the second-order LDP for the 0° direction at $(3, 3)$. First, the first-order derivative bits are calculated at the center pixel and top-left adjacent pixel along the 0° direction, as shown in the left-uppermost case of Fig. 9. I_4 and I_c of the center pixel are 8 and 2, and I_4 and I_c of the top-left adjacent pixel are 5 and 7. Therefore, the first-order derivative bits of the center pixel and top-left adjacent pixel are 1 and 0, respectively, and the result of their exclusive-OR operation is 1. Similar to this method, the first-order derivative bits between the center pixel and adjacent pixels are compared in the clockwise direction, and 8 bits for the 0° direction are extracted, as shown in Fig. 9. Consequently, 32 bits per pixel are extracted for the four directions of 0° , 45° , 90° , and 135° . The finger-vein code of 28,672 ($56 \times 16 \times 32$) bits is produced from the sub-sampled image of 60×20 pixels. Four rows and four columns are excluded at the image border because the first-order derivative bits cannot be calculated at an image border.

The score of the finger-vein recognition is finally measured by calculating the hamming distance (HD) between the finger-vein codes of the enrolled and those of input images as

$$HD = \frac{1}{N} \|codeA \otimes codeB\|, \quad (10)$$

where $code A$ and $code B$ denote the finger-vein codes of the enrolled and input images, respectively. N denotes the number of bits of finger-vein codes.

2.6 Fingerprint Recognition Based on LDP

The ridge quality of the fingerprint image by the proposed device is not as good as that by a conventional 2D fingerprint sensor because the image is acquired without touching the sensor, as shown in Fig. 1. Therefore, the errors of detecting ridge and minutia points are great, which degrades the consequent accuracy of fingerprint recognition (see Figs. 18

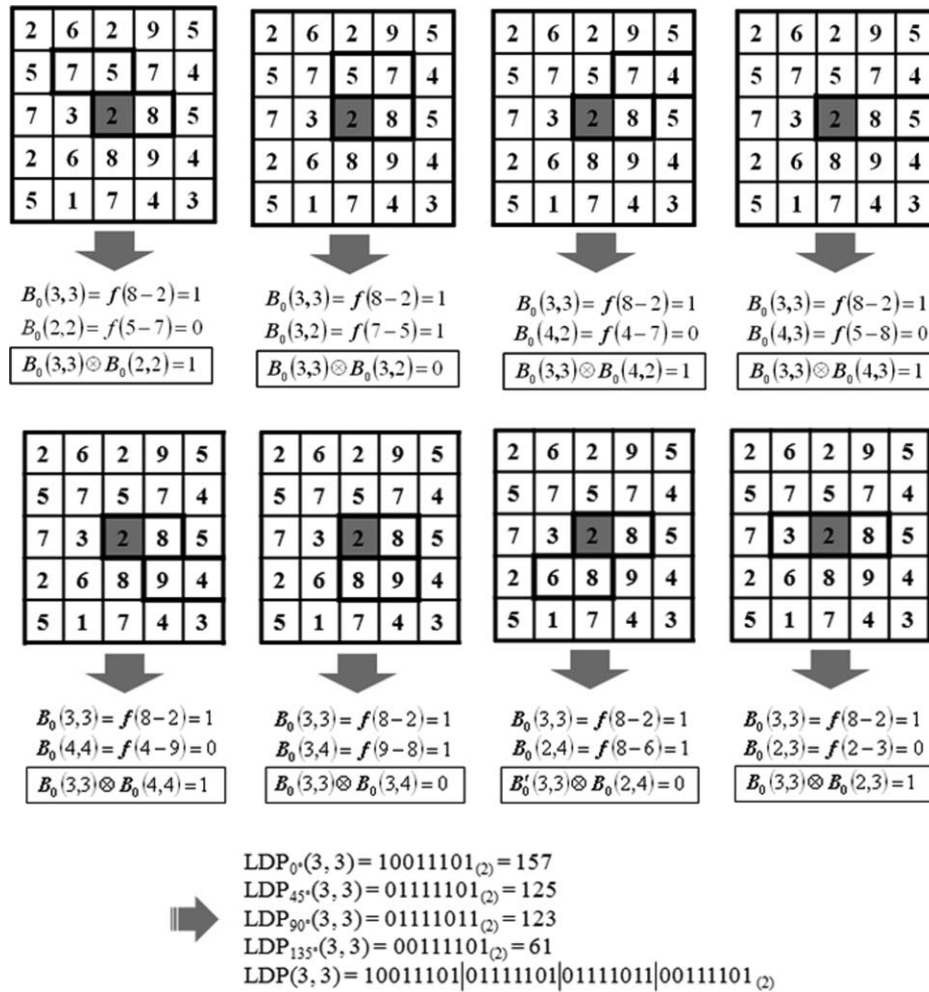


Fig. 9 Example of the LDP method.

and 19). We propose LDP-based fingerprint recognition to counteract this problem.

Figure 10 shows the overall process for fingerprint recognition. First, the fingerprint region is selected, as shown in Fig. 11. The center of the fingerprint region is determined by the medial point between the upper and lower boundaries of the detected finger region at each x position, which is as distant as L pixels from the fingertip. Here, the upper and lower boundaries of the finger region and fingertip are detected by the method presented in Fig. 3.

The width and height of the fingerprint region are determined by half of the finger thickness at the medial point. The finger thickness is defined as the distance between the upper and lower boundaries of the finger region. In order to extract fingerprint codes that are robust to the size variations caused by changes in the Z distance between the camera and user's

finger, the L value of Fig. 11 is adaptively determined as two-thirds of the average finger thickness. The fingerprint region is also normalized into 40×40 pixels to reduce computation time and image noise.

The fingerprint codes are extracted by the LDP method in the same manner as finger-vein recognition. The repetitive feature codes of fingerprint are extracted from the continuative edges between the valley and ridge. In this study, four histograms were obtained from the decimal values of the fingerprint codes in four directions (0° , 45° , 90° , and 135° , as shown in Fig. 9), and the dissimilarity score was then calculated by the chi square distance (CSD) between the histograms of the enrolled and input images as²⁰

$$CSD = \frac{1}{2} \sum_{i=0}^{255} \frac{[histoA_\alpha(i) - histoB_\alpha(i)]^2}{histoA_\alpha(i) + histoB_\alpha(i)}$$

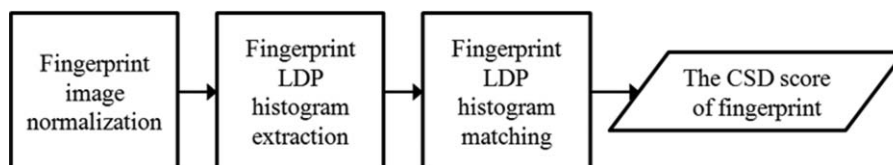


Fig. 10 Flowchart of the finger print recognition method.

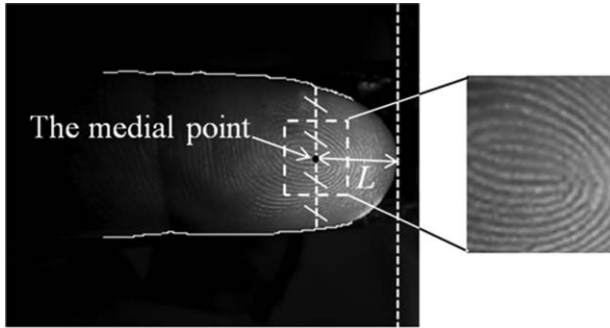


Fig. 11 Example of the fingerprint region detection.

$$\alpha = 0^\circ, 45^\circ, 90^\circ, 135^\circ, \quad (11)$$

where $histoA_\alpha(i)$ and $histoB_\alpha(i)$ denote the histograms of the decimal values for the LDP codes of the enrolled and input images, respectively. A small positional difference in the enrolled and input images can cause great intra-variation because the fingerprint has a fine structure of ridges, and the local matching based on the HD of Eq. (10) cannot solve this problem. Thus, we use the histogram-based matching of Eq. (11), which is global matching and insensitive to small positional differences.

The finger veins exist sparsely, as shown in Fig. 7, and are more insensitive to the positional differences than fingerprint ridges. Thus, HD-based matching is used for finger-vein recognition, as shown in Eq. (10).

2.7 Finger Geometry Recognition Based on FD and PCA

The procedure for finger geometry recognition is presented in Fig. 12. In previous works, the Fourier descriptor (FD) of the finger thickness was used for the finger geometry features.³

The FDs represent the shape of a single finger in the frequency domain; the descriptors of the low frequency components represent the global shape, and the descriptors of the high frequency components represent the detailed shape. After measuring the finger thicknesses t_i of the finger region, as shown in Fig. 13, they are transformed into the frequency domain by using a fast Fourier transform.³ In addition, G is the vector of the FDs, which consists of the magnitudes of the frequency components, and is given as

$$G = \begin{bmatrix} |T_1| & \dots & |T_{n-1}| \\ |T_0| & \dots & |T_0| \end{bmatrix}, \quad (12)$$

where T_i and T_0 denote the i th component in the frequency domain and DC component, respectively. The scale invariant geometry features can be extracted by dividing the frequency components by the DC component.³ In this study, the number of finger thickness features was 512, so 511 FDs were used for the finger geometry recognition. In a previous study,³

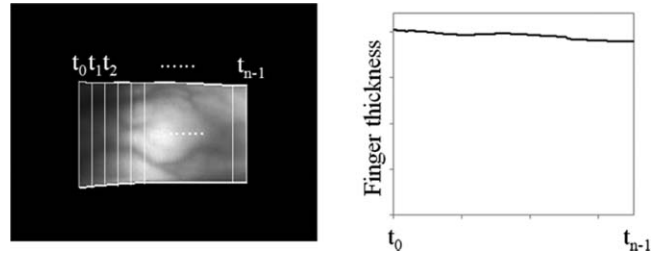


Fig. 13 Example of the finger geometry feature based on the finger thickness.^{2,3}

finger geometry features based on FDs were obtained using these methods.

However, the accuracy of the finger geometry recognition in Ref. 3 can be enhanced because orthogonality between the FDs is not guaranteed. Thus, PCA is used. The so-called scatter matrix S is calculated as²¹

$$S = \sum_{i=1}^N [G_i - \bar{G}] [G_i - \bar{G}]^T, \quad (13)$$

where \bar{G} denotes the mean vector of the FDs on the training dataset. The eigenvector e_i and eigenvalue λ_i are obtained by

$$S e_i = \lambda_i e_i, \quad i = 1, 2, \dots, N. \quad (14)$$

The score of the finger geometry recognition is finally measured by calculating the Euclidean distance (ED) between the eigenvalues of the enrolled and input FDs as

$$ED = \frac{1}{m-1} \sqrt{\|\lambda_A - \lambda_B\|^2}, \quad (15)$$

where λ_A and λ_B denote the vectors of eigenvalues of the enrolled and input FDs, respectively. m denotes the number of eigenvalues.

2.8 Fuzzy Score Normalization

The scores of the finger-vein, fingerprint, and finger geometry recognition are normalized by the proposed fuzzy score normalization. This technique provides an attribute value that represents the degree of membership in a specific class.²² On the basis of this value, the degree of membership is newly proposed as

$$h' = \frac{1}{1 + e^{\frac{h - (\mu_g + \mu_i)/2}{\max(\sigma_g, \sigma_i)/2}}}, \quad (16)$$

where μ_g and σ_g denote the mean and standard deviation of the genuine class, respectively. μ_i and σ_i are the mean and standard deviation of the imposter class, respectively.

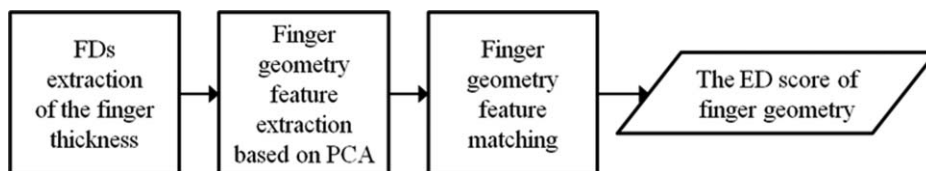


Fig. 12 Flowchart of the finger geometry recognition method.

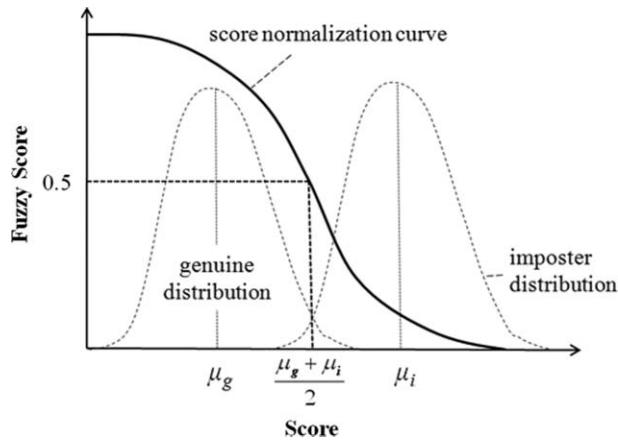


Fig. 14 Proposed fuzzy score normalization.

The genuine input data show lower distances [Eqs. (10), (11), and (15)] with the enrolled data by finger-vein, fingerprint, and finger geometry recognition. The imposter data show higher distances. On the basis of these facts, we design a fuzzy membership function for score normalization, as shown in Fig. 14.

After obtaining the genuine and imposter classes with training data, the score (distance) belonging to the genuine class is forced to be 1, and that to the imposter class is 0 through the membership function. Through normalization of each score (distance) of the finger-vein, fingerprint, and finger geometry recognition by using three membership functions,

the separation of the genuine and imposter classes can be increased, which reduces the consequent equal error rate (EER) of recognition.

The normalized score is set to 0.5 at the center of the means (μ_g and μ_i) of the genuine and imposter distributions, as shown in Fig. 14, and the gradient of the score normalization curve is controlled by the two standard deviations (σ_g and σ_i) of the genuine and imposter distributions. Smaller standard deviations make the curve steep and vice versa.

2.9 Score-Level Fusion and Classification

The three normalized scores are used as the inputs of the SVM, which finds the optimal decision hyperplane in terms of maximizing the distances between the support vectors.^{21,23,24} A three-dimensional SVM requires a great number of samples and has higher complexity than a two-dimensional SVM. Thus, we divided the problem into three SVMs that use two scores for inputs, as shown in Fig. 15; the three decision values obtained from the three SVMs were then combined using a weighted SUM rule. In our experiments, the optimal decision hyperplanes of the SVMs were determined by a radial basis function (RBF) kernel (with a γ value of 1) among the five kernels tested: the dot, polynomial, RBF, neural, and ANOVA kernels.

3 Experimental Results

3.1 Databases

There is no public database in which finger-vein and fingerprint images have been captured at the same time, so finger-vein and fingerprint images were collected with the

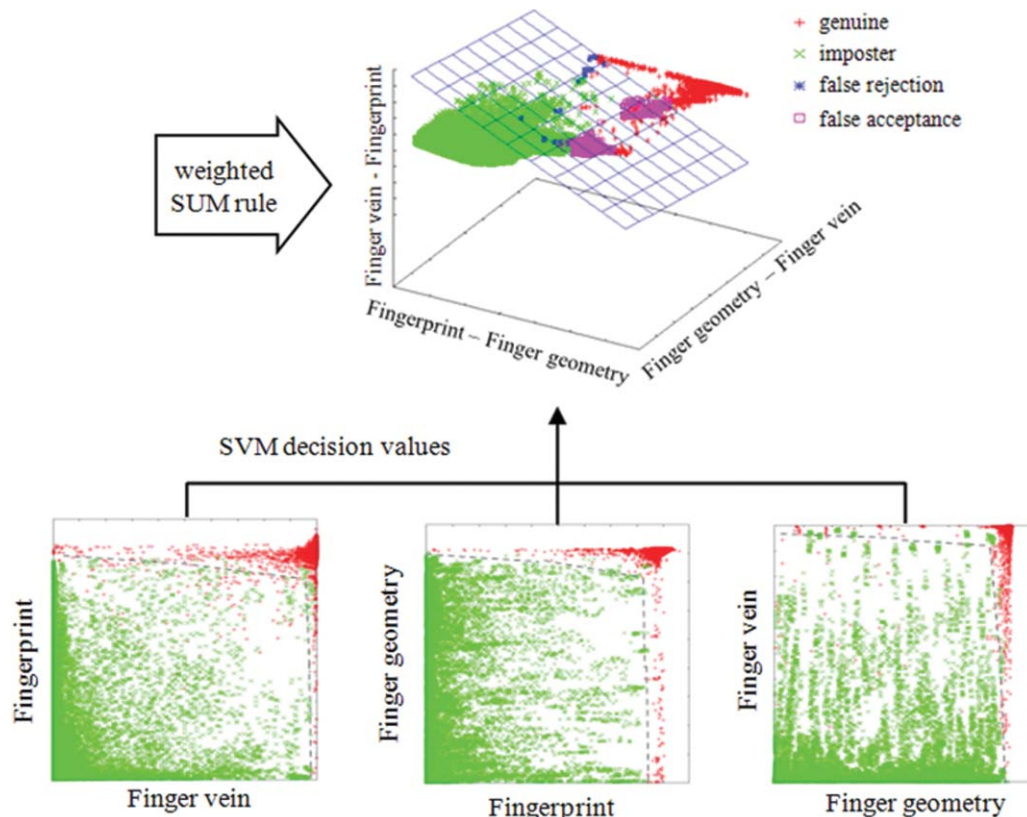


Fig. 15 Score-level fusion and classification.

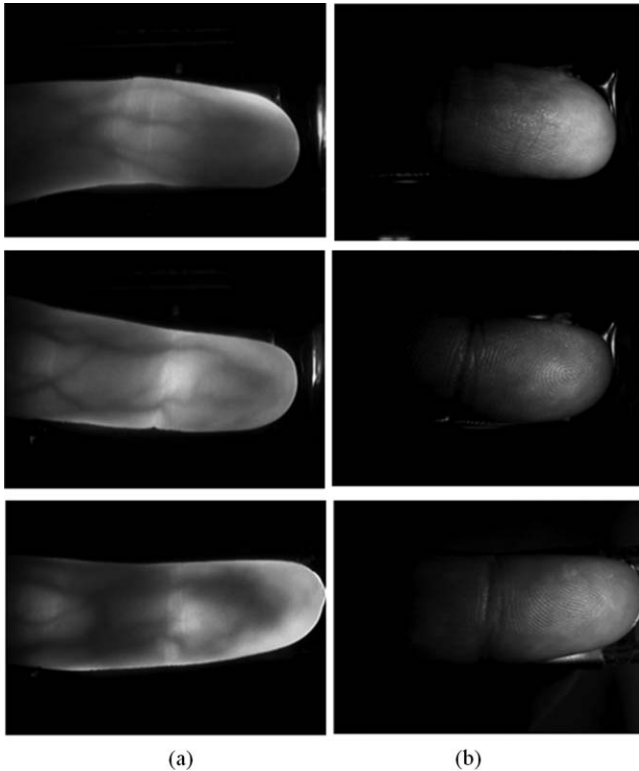


Fig. 16 Images on the collected database: (a) finger-vein images and (b) fingerprint images.

capturing device shown in Fig. 1. The database consists of 6380 finger-vein images and 6380 fingerprint images; these were acquired from eight fingers of 80 people. Nine to 10 finger-vein images and fingerprint images were simultane-

ously captured per each finger. It was difficult to capture the thumb image by the proposed capturing device. The veins of the thumb are not clear because the NIR light barely penetrates the skin of the thick thumb. The thumb is not used in other commercial systems either.^{12,25} The resolution of the finger-vein and fingerprint images was 640×480 pixels with an 8-bit gray level. Figure 16 shows examples of the database images.

3.2 Comparisons of the Different Types of Approaches for Finger-Vein Recognition

The performances of different types of approaches for finger-vein recognition were compared in terms of recognition accuracy. Using the LBP and LDP methods, the finger-vein codes were extracted from the normalized images obtained in the preprocessing step. We then measured the similarity between the codes of the input image and those of the enrolled ones using two types of methods: one calculated the HD from the finger-vein codes, and the other calculated the CSD from the histograms of the finger-vein codes.

Figure 17 shows the ROC curves obtained from the four different types of approaches for finger-vein recognition. The ROC curve indicates the genuine acceptance rate (GAR) at various levels of false acceptance rates (FAR). The GAR is defined as $100 - \text{FRR} (\%)$. FRR is the false rejection rate, which is the error rate of falsely rejecting the enrolled (genuine) code as an un-enrolled (imposter) one. FAR is the error rate of falsely accepting the unenrolled (imposter) code as the enrolled (genuine) one.

The approach calculating the HD between the finger-vein codes extracted by the LDP method produced the best results, as shown in Fig. 17. Because a human finger does not have repetitive and fine vein patterns, as shown in Fig. 7, the intra-variations caused by the positional differences between the input and enrolled image are not great. Thus, the local

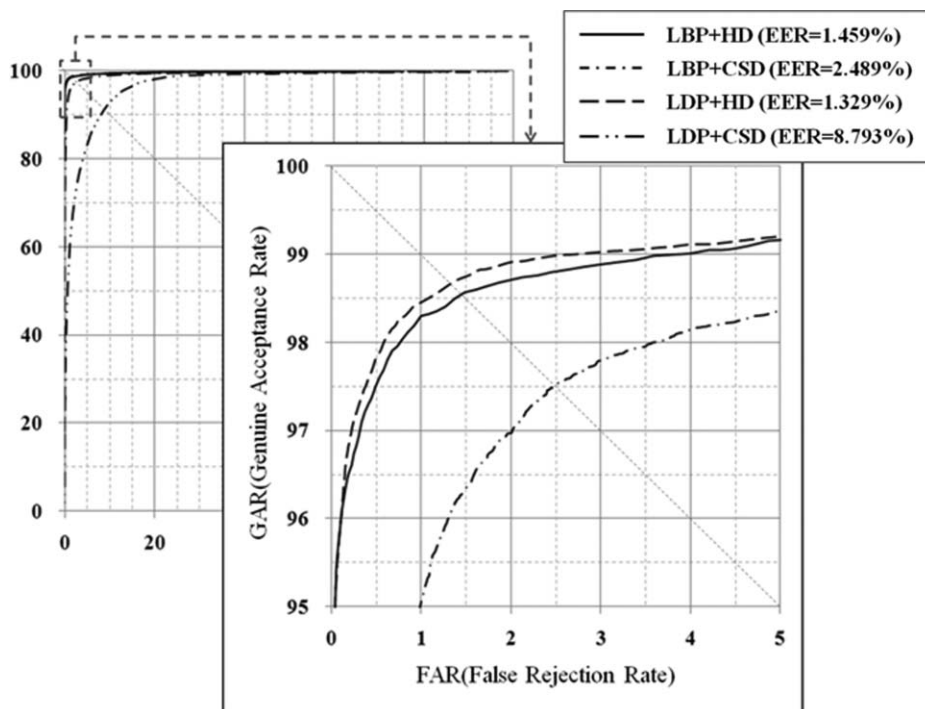


Fig. 17 ROC curves of various finger-vein recognition methods on 6380 finger-vein images.

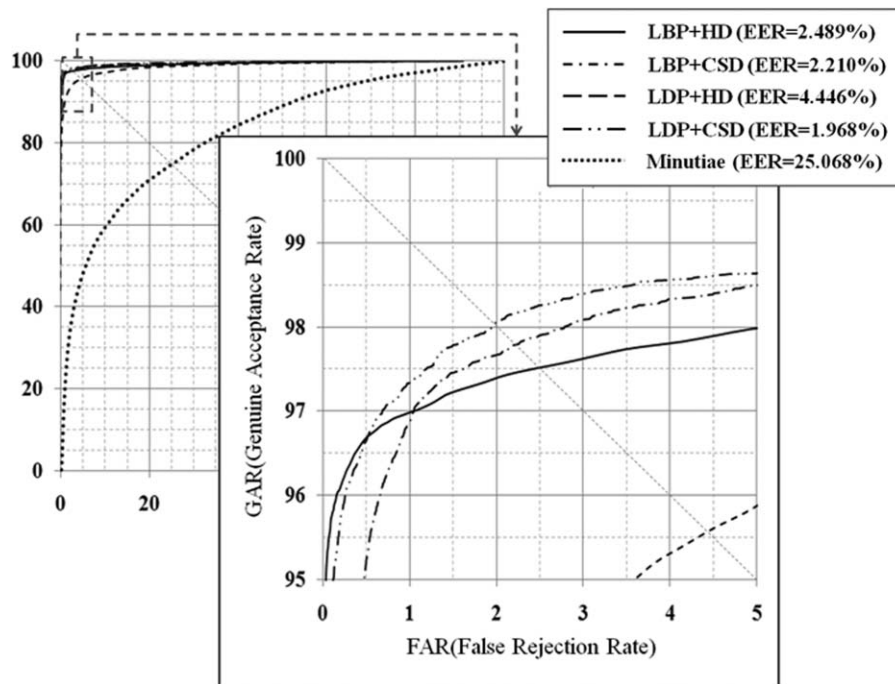


Fig. 18 ROC curves of various fingerprint recognition methods on 6380 fingerprint images.

matching using the HD between the binary finger-vein codes [Eq. (10)] performed better than global matching using the CSD between histograms [Eq. (11)].

3.3 Comparisons of the Different Types of Approaches for Fingerprint Recognition

The performances of the different types of approaches for fingerprint recognition were compared in the same manner as the finger-vein recognition methods. As shown in Fig. 18, the recognition accuracy of calculating the CSD between the histograms of the fingerprint codes extracted by the LDP method was better than the other methods.

Because a human fingerprint consists of repetitive and fine patterns of ridges and valleys—unlike finger veins—the intra-variations caused by the positional differences between the input and enrolled image can be great. Thus, global matching using the CSD between histograms [Eq. (11)] performed better than local matching using the HD [Eq. (10)] between binary fingerprint codes. The ridge quality of the fingerprint image by the proposed device is not as good as that by the conventional 2D fingerprint sensor because the image is acquired without touching on the sensor, as shown in Fig. 1. Thus, the errors in detecting ridge and minutia points are great, which degrades the consequent accuracy of fingerprint recognition.

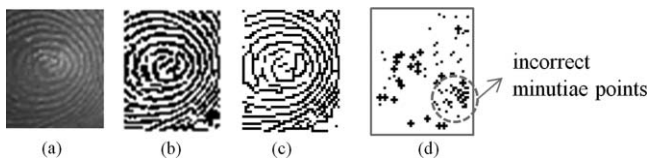


Fig. 19 Example of fingerprint line segmentation: (a) original image; (b) segmented image; (c) skeleton image; and (d) detected minutia points (cross = ending points, dots = bifurcation points).

The ROC curve of the minutiae-based fingerprint recognition was measured by calculating the modified Hausdorff distance after detecting minutia points with local binarization and thinning algorithm. As shown in Fig. 19, many minutia points are incorrectly detected because fingerprint images with bad quality are captured owing to touchless acquisition, illumination variation, and image noises. Thus, the performance of the minutiae-based fingerprint recognition was not good, as shown in Fig. 18.

3.4 Comparisons of the Different Types of Approaches for Finger Geometry Recognition

The performance of the proposed approach combining the FD and PCA methods was compared with those of the previous approach that used only the FD method.³ In our experiment, 1276 finger images were used to train the PCA, and the other images were used to measure the recognition accuracy.

In order to determine the optimal number of eigenvectors, we measured the recognition accuracy (100 – EER) according to the number of eigenvectors, as shown in Fig. 20. The best recognition accuracy of 98.56% was produced when using four eigenvectors. There were no great variations in the recognition accuracy when more than four eigenvectors was used, and the recognition accuracy was actually 97.21% when all 511 eigenvectors were used. We measured the recognition accuracy of the proposed approach on the test set of 5104 images. As shown in Fig. 21, the EER of the proposed method was reduced by 3.191% (4.634% – 1.443%) over the previous method that used only the FD found in Ref. 3.

3.5 Comparisons of Score Normalization Methods

The performance of the fuzzy score normalization method was evaluated by comparing it to the Z-score normalization method on the fusion method with the SUM rule. The

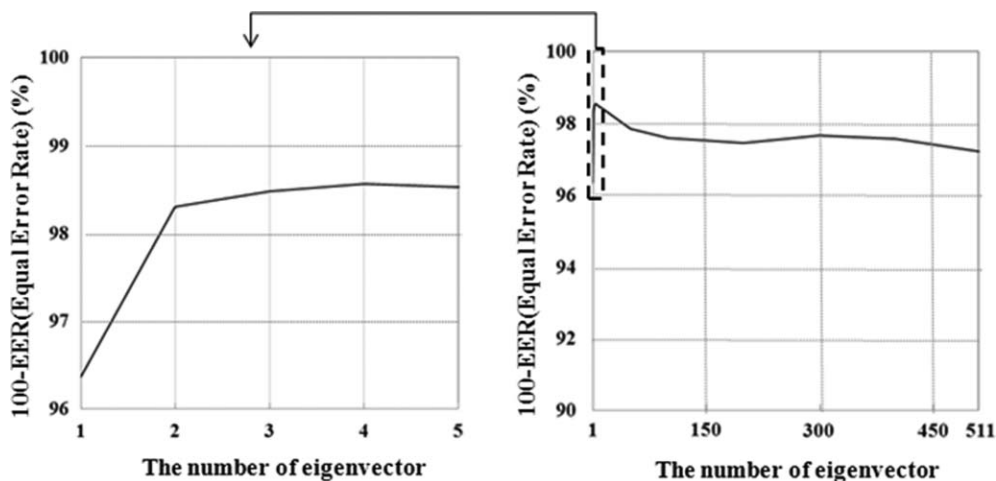


Fig. 20 Recognition accuracy according to the number of eigenvectors.

Z-score normalization method uses the arithmetic mean μ and standard deviation σ of the data distribution as ²⁶

$$h'' = \frac{h - \mu}{\sigma}. \tag{17}$$

Training data are required for the parameter selection in both the proposed score normalization method and Z-score normalization method. Therefore, we selected 3190 training images randomly and measured the recognition accuracy with the remaining images. The average recognition accuracy was measured from the test performed 10 times, and the SUM rule was used for the fusion of the normalized scores. The SUM rule determines a final score by the sum of the scores obtained from each method. As shown in Fig. 22 and Table 1, we obtained the following observations:

- (i) The EER of the proposed score normalization method was reduced by 0.469% (1.243% – 0.774%) over the Z-score normalization method.
- (ii) The difference between the minimum and maximum EERs was smaller in the proposed method than in the Z-score normalization method.

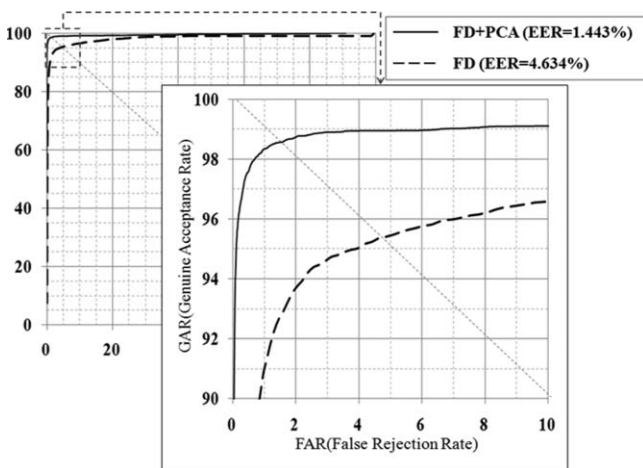


Fig. 21 ROC curves of the approaches for the finger geometry recognition on the test set of 5104 images.

Therefore, we found that the proposed method achieves a more stable and efficient score fusion than the Z-score normalization method.

3.6 Comparisons of the Multimodal and Unimodal Recognition Approaches

We compared the unimodal and multimodal recognition approaches that fused the scores with the SVM. For five iterations, we randomly selected 3190 images to train the SVM and measured the recognition accuracy with the remaining images. The fusion of the finger veins (FV), fingerprints (FP), and finger geometry (FG) was achieved by the proposed method, which combined the decision values obtained from the three SVMs by the weighted SUM rule. As shown in Fig. 23, all of the multimodal recognition approaches outperformed the unimodal recognition approaches, and the fusion of the three scores produced the best results. We found that using various biometric features in conjunction leads to a high recognition accuracy.

The processing time of the proposed method was measured on a desktop computer with an Intel Core Quad CPU 2.66 GHz. It took 79.0, 18.7, and 0.9 ms for the detections of the finger region and fingertip, rotation alignment, and size normalization, respectively. The processing times for the LDP-based finger vein and the LDP-based fingerprint recognition were 0.4 and 0.3 ms, respectively. The finger geometry recognition took 2.3 ms. In addition, it took about 3.1 ms for the score level fusion, including the fuzzy score normalization and SVM classification. Consequently, the total processing time of the proposed multimodal method was almost 104.7 (79.0 + 18.7 + 0.9 + 0.4 + 0.3

Table 1 Recognition accuracy for different types of score normalization methods.

Methods	EER (%)		
	Min	Max	Average
Fuzzy score normalization	0.458	0.959	0.774
Z-score normalization	0.461	1.394	1.243

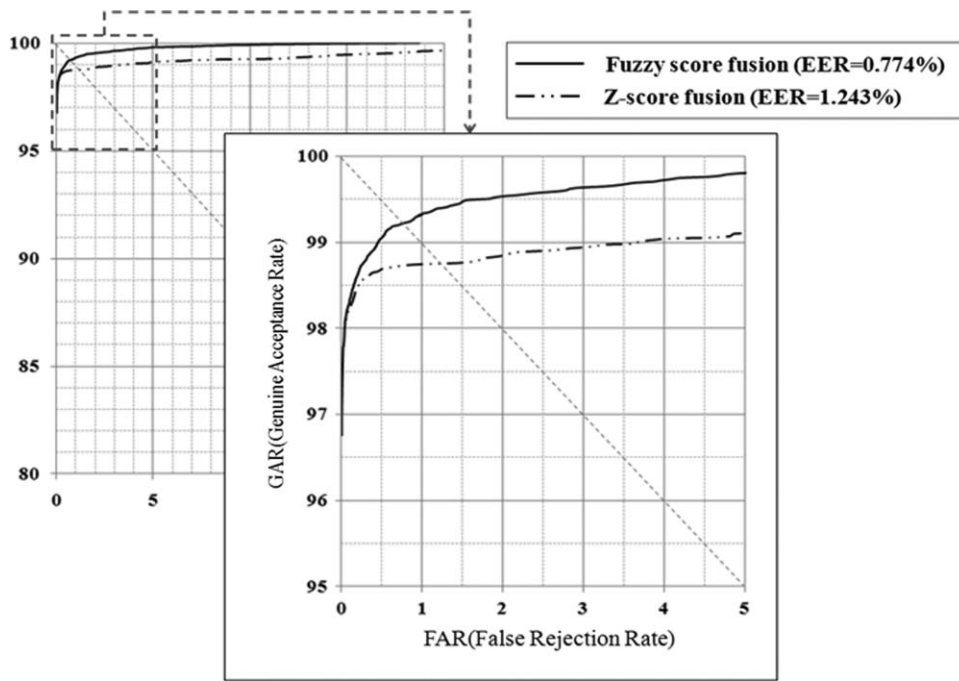


Fig. 22 ROC curves of the different types of score normalization.

+ 2.3 + 3.1) ms on average, whereas those of the finger vein, fingerprint, and finger geometry recognitions were 99.0 (79.0 + 18.7 + 0.9 + 0.4), 98.9 (79.0 + 18.7 + 0.9 + 0.3), and 100.9 (79.0 + 18.7 + 0.9 + 2.3) ms, respectively.

Thus, we confirmed that the processing time of the proposed multimodal method is a little longer than those of finger vein, fingerprint and finger geometry recognitions by 5.7 (104.7 – 99.0), 5.8 (104.7 – 98.9) and 3.8 (104.7 – 100.9) ms, respectively, because the unimodal biometric methods also need preprocessing, including the detections of the finger

region and fingertip, rotation alignment, and size normalization.

3.7 Comparisons of the Proposed Fusion and Other Fusion Rules

The performance of the proposed fusion method was compared with various fusion rules such as MAX, MEDIAN, MIN, and SUM rules. The MAX, MEDIAN, and MIN rules respectively represent the fusion methods that determine the

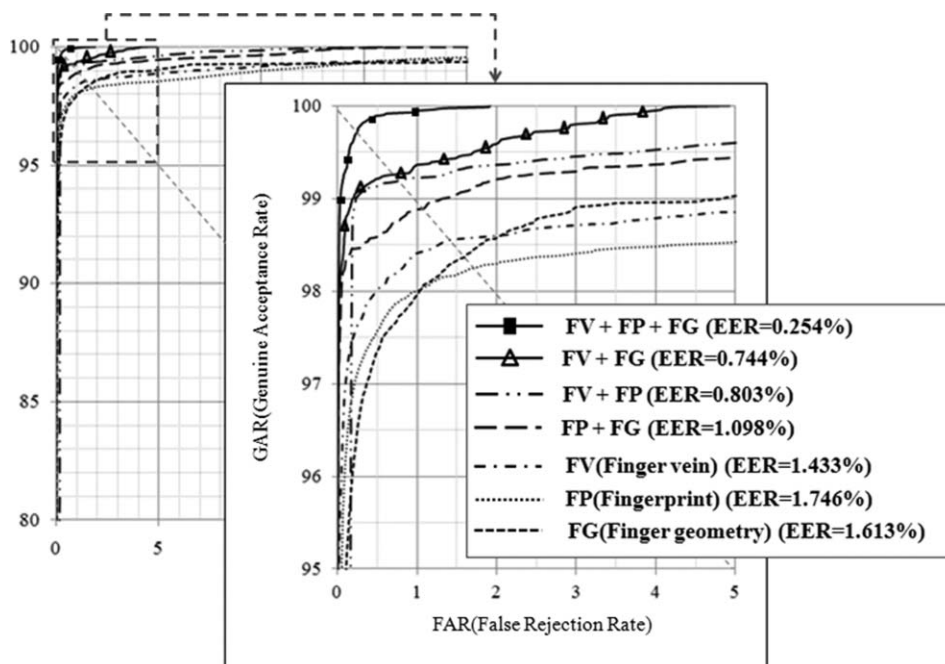


Fig. 23 ROC curves of the unimodal and multimodal recognition approaches using the SVM.

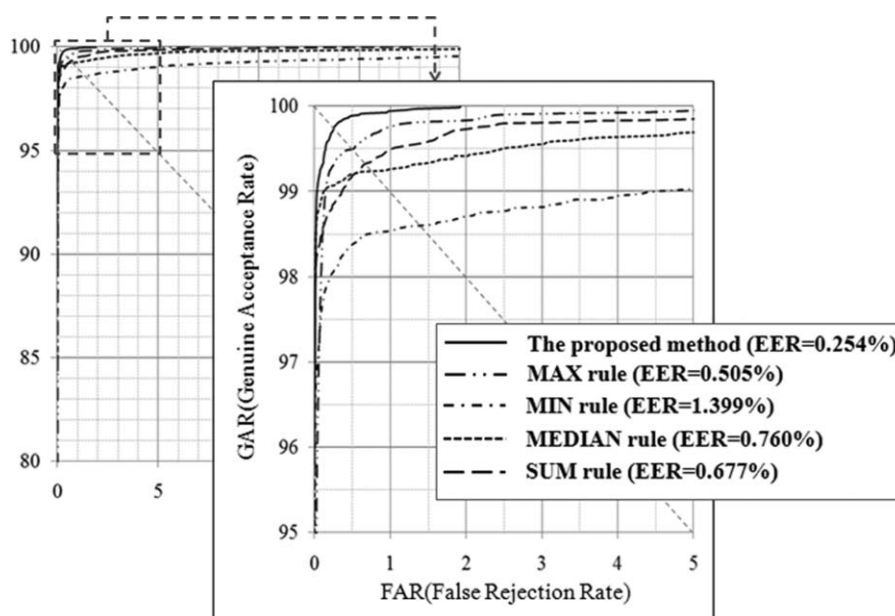


Fig. 24 ROC curves of the fusion methods using the various rules.

final score by selecting the maximum, median, and minimum score from the recognition approaches. The average recognition accuracy was measured on the dataset excluding 3190 training images and using five iterations. As shown in Fig. 24, the proposed fusion method outperformed the other fusion methods because the proposed method effectively discriminates between the genuine and imposter classes by using the SVM.

4 Conclusion

This paper proposes a finger recognition approach based on the score-level fusion of the finger-vein, fingerprint, and finger geometry features. The performances of the finger-vein and fingerprint recognition were improved by using LDP, and the performance of the finger geometry recognition was greatly improved by combining the FDs with the PCA methods. A fuzzy score normalization was introduced, and we combined the three decision values obtained from three two-dimensional SVMs in order to reduce the complexity inherent to three-dimensional SVM. Consequently, the proposed finger recognition had high recognition accuracy owing to the use of the various biometric features. However, the performance of the proposed approach can deteriorate by severe rolling and bending of the finger; therefore, we will study finger recognition that is robust to rolling and bending fingers in future work.

Acknowledgments

This study was supported by a grant of the Korea Healthcare technology R&D Project, Ministry of Health & Welfare, Republic of Korea (A102058).

References

1. A. K. Jain, A. Ross, and S. Prabhakar, "An introduction to biometric recognition," *IEEE Trans. Circuits Syst. Video Technol.* **14**(1), 4–19 (2004).

2. B. J. Kang and K. R. Park, "Multimodal biometric authentication based on the fusion of finger vein and finger geometry," *Opt. Eng.* **48**(9), 090501 (2009).
3. B. J. Kang and K. R. Park, "Multimodal biometric method based on vein and geometry of a single finger," *IET Computer Vis.* **4**(3), 209–217 (2010).
4. N. Miura, A. Nagasaka, and T. Miyatake, "Extraction of finger-vein patterns using maximum curvature points in image profiles," *IEICE Trans. Inf. Syst.* **E90-D**(8), 1185–1194 (2007).
5. R. Snelick, U. Uludag, A. Mink, M. Indovina, and A. Jain, "Large scale evaluation of multimodal biometric authentication using state-of-the-art system," *IEEE Trans. Pattern Anal. Mach. Intell.* **27**(3), 450–455 (2005).
6. M. Tico and P. Kuosmanen, "Fingerprint matching using an orientation based minutia descriptor," *IEEE Trans. Pattern Anal. Mach. Intell.* **25**(8), 1009–1014 (2003).
7. L. Sha and X. Tang, "Orientation-improved minutiae for fingerprint matching," in *Proc. 17th Int. Conf. on Pattern Recognition*, vol. **4**, pp. 432–435 (Cambridge, UK: IEEE Computer Society, 2004).
8. K. Lee and S. Parabhakar, "Probabilistic orientation field estimation for fingerprint enhancement and verification," in *Proc. Biometric Symposium*, pp. 41–46 (Tampa, Florida, USA: IEEE Computer Society, 2008).
9. J. Qi, S. Yang, and Y. Wang, "Fingerprint matching combining the global orientation field with minutia," *Pattern Recogn. Lett.* **26**(15), 2424–2430 (2005).
10. E. C. Lee, H. C. Lee, and K. R. Park, "Finger vein recognition by using minutia based alignment and local binary pattern-based feature extraction," *Int. J. Imaging Syst. Technol.* **19**(3), 179–186 (2009).
11. H. C. Lee, B. J. Kang, E. C. Lee, and K. R. Park, "Finger vein recognition by using weighted LBP code based on SVM," *J. Zhejiang Univ.-Sci. C*, **11**(7), 514–524 (2010).
12. J. Hashimoto, "Finger vein authentication technology and its future," in *Proc. Symposium on VLSI Circuits*, pp. 5–8 (Honolulu, Hawaii, USA: IEEE Electron Devices Society, 2006).
13. M. A. Ferrer, A. Morales, and L. Ortega, "Infrared hand dorsum images for identification," *Electron. Lett.* **45**(6), 306–308 (2009).
14. B. Zhang, Y. Gao, S. Zhao, and J. Liu, "Local derivative pattern versus local binary pattern: face recognition with high-order local pattern descriptor," *IEEE Trans. Image Process.* **19**(2), 533–544 (2010).
15. H. C. Lee, K. R. Park, B. J. Kang, and S. Park, "A new mobile multimodal biometric device integrating finger vein and fingerprint," in *Proc. 4th Int. Conf. on Ubiquitous Information Technologies and Applications*, pp. 307–310 (Fukuoka, Japan: IEEE, 2009).
16. L. Wang and G. Leedham, "Near- and far- infrared imaging for vein pattern biometrics," in *Proc. IEEE International Conference on Video*

- and *Signal Based Surveillance*, pp. 52 (Sydney, Australia, IEEE Computer Society, 2006).
17. Logitech QuickCam, <http://www.logitech.com/>, accessed October 25, 2010.
 18. T. Ojala, M. Pietikäinen, and D. Harwood, "A comparative study of texture measures with classification based on feature distributions," *Pattern Recogn.* **29**(1), 51–59 (1996).
 19. T. Ojala, M. Pietikäinen, and T. Maenpää, "Multiresolution gray-scale and rotation invariant texture classification with local binary patterns," *IEEE Trans. Pattern Anal. Mach. Intell.* **24**(7), 971–987 (2002).
 20. P. Suau, "Robust artificial landmark recognition using polar histograms," *Lect. Notes Comput. Sci. on IROBOT* **3808**, 455–461 (2005).
 21. R. O. Duda, P. E. Hart, and D. G. Stork, *Pattern Classification*, Wiley-Interscience Publication (2001).
 22. W. Au and K. C. Chan, "Classification with degree of membership: a fuzzy approach," in *Proc. IEEE International Conference on Data Mining*, pp. 35–42 (San Jose, California, USA. IEEE Computer Society, 2001).
 23. M. S. Fahmy, A. F. Atiya, and R.S. Elfouly, "Biometric fusion using enhanced SVM classification," in *Proc. International Conference on Intelligent Information Hiding and Multimedia Signal Processing*, pp. 1043–1048 (Los Alamitos, USA. IEEE Computer Society, 2008).
 24. V. Vapnik, *Statistical Learning Theory*, Wiley-Interscience (1998).
 25. Finger Vein Reader, <http://www.hitachi-omron-ts.com/products/fingervein/index.html>, accessed October 25, 2010.
 26. A. K. Jain, K. Nandakumar, and A. Ross "Score normalization in multimodal biometric systems," *Pattern Recogn.* **38**(12), 2270–2285 (2005).



Byung Jun Kang received his BS and MS degrees in Software and Computer Science from Sangmyung University, Seoul, South Korea, in 2004 and 2006, respectively. In 2009, he also earned a PhD in Computer Science from the Department of Computer Science, Sangmyung University, Seoul, South Korea. He was a senior researcher at the Electronics and Telecommunications Research Institute from May 2009 to August 2010. He is a senior researcher in the Technical Research Institute at Hyundai Mobis. His research interests include biometrics, image processing, and advanced safety vehicles.



Kang Ryoung Park received his BS and MS degrees in Electronic Engineering from Yonsei University, Seoul, Korea, in 1994 and 1996, respectively. He also received his PhD in Computer Vision from the Department of Electrical and Computer Engineering, Yonsei University, in 2000. He was an assistant professor in the Division of Digital Media Technology at Sangmyung University from March 2003 to February 2008. He has been an assistant and associate professor in the Division of Electronics and Electrical Engineering at Dongguk University since March 2008. He is also a research member of BERC. His research interests include computer vision, image processing, and biometrics.



Jang-Hee Yoo received his BSc degree in physics from HUFs in 1988, his MSc degree in computer science from HUFs, S. Korea, in 1990. He received his PhD in electronics and computer science from the University of Southampton, UK, in 2004. Since November 1989, he has been with Electronics and Telecommunication Research Institute (ETRI), S. Korea as a principal member of research staff. His current research interests include embedded computer vision, biometric systems, human motion analysis, intelligent video surveillance, HCI and intelligent robot. He is a member of IEEE and IEEK.



Jeong Nyeo Kim received his BSc degree from Chonnam National University in 1987, his MSc degree in Computer Eng. from Chungnam National University, S. Korea, in 2000. He received his PhD in Computer Eng. from Chungnam National University, in 2004. Since February 1988, he has been with Electronics and Telecommunication Research Institute (ETRI), S. Korea. His current research interests include system & network security, security OS, and biometrics.